Nuclear Physics A462 (1987) 751–780
North-Holland, Amsterdam

PROTON–NUCLEUS INTERACTION AT HIGH ENERGY

J. CUGNON

Institut de Physique B5, Université de Liège, Sart Tilman, B-4000 Liège 1, Belgium

Received 6 August 1986

Abstract: The interaction of high energy protons (between 100 MeV and 20 GeV incident energy) with nuclei is studied in the frame of an intranuclear cascade (INC) model. Particular attention is paid to the energy loss of the projectile and on the emission patterns. It is shown that, in general, the incident proton has left the nucleus before the emission process starts. The latter proceeds first on a rather short time scale and involves fast particles. Progressively the emission rate slows down and the ejected particles are less rapid. The target mass, energy and impact parameter dependences of the energy loss is displayed. As a by-product, we calculate the nuclear stopping power. We investigate the fluctuations in the number of primary collisions, i.e. those suffered by the incoming nucleon, and in the energy loss. Fluctuations in the number of ejectiles are also studied as well as the relationship between primary collisions and the number of fast (grey) particles. The latter number is tentatively related with the number of site vacancies in percolation models. The entropy created inside the target is also calculated. It is shown that the representative point of the system in the (internal energy, entropy) plane spends a relatively long time in the coexistence zone and even in the instability zone corresponding to gas-liquid transition. Implications for these two models of fragmentation are discussed. A preliminary comparison with energy loss measurements in the 3–4 GeV/c range is performed.

1. Introduction

The interaction of high energy protons with atomic nuclei has attracted the attention for many years [1]. But the main emphasis was put on coherent elastic and inelastic scattering and on the understanding of these processes in terms of multiple scattering series [2] (or more recently in terms of scattering by relativistic scalar and vector average fields [3])). In recent years however, there has been among physicists an increasing interest in the more violent (and mainly incoherent) processes which are taking place in these reactions. The target nucleus can undergo some transformations. In some cases, it loses a few nucleons (the so-called spallation). If the excitation energy is sufficiently high, it can presumably disintegrate into many pieces.

It is a general belief that, in a first approximation, the interaction process between an incoming proton with an energy of a few hundreds of MeV or more can be grossly divided in two steps. In the first rapid step, the incoming nucleon makes a few (mainly) incoherent scatterings with nucleons of the target, depositing in this way some fraction of its energy. The second step, which supposedly starts after the incoming proton has left the target, involves the propagation and the dissipation of the energy gained by the nucleus. Generally, the ultimate fate of the nucleus is

its fragmentation. The mass yield has been measured in many circumstances and exhibits a so-called U-shape [4]): the small fragments and those of size comparable with the original nucleus are the more represented. But, any fragment between the nucleon and the target has been observed.

Not very much is known about the second step and only several idealizations have been proposed. Let us summarize the most important ones.

(i) "Spallation" models [5]): the energy is evacuated by the nucleons hit in the first step, which leave the nucleus without interaction. Possibly, the remaining nucleus releases some energy gained by its deformation.

(ii) Thermal models [6,7]): the energy is shared by the whole nucleus which decays in fragments according the phase space constituted by the possible partitions of the target. These models involve at least one free parameter which can be considered as the freeze-out density.

(iii) "Cold fragmentation" [8]). Those models share with the previous ones the idea of equipopulation of a phase space. But here, the phase space is restricted to the possible fragmentations including neither the relative motion between the fragments nor the intrinsic excitation of the fragments.

(iv) "Condensation models" [9-11]). As thermal models, the latter assume a thermalization of the system, but the separation into fragments is determined by the proximity of the critical point of the underlying gas-liquid transition.

(v) "Percolation" models [12-14]). In the latter, it is assumed that the eventual fragmentation of the nucleus is determined by the geometry of the "damage" made to the nucleus after the initial step which, in turn, is believed to be largely correlated to the number of nucleons hit during the first step.

Another aspect of the fragmentation is the comparative size of the fragments. It is generally believed that the peripheral (soft) collisions produce a big fragment and several small ones. On the other hand, violent (central) collisions are expected to produce many fragments of comparable size, and, of course, of much smaller size than the original nucleus (the so-called multifragmentation). This possibility is absent from model (i). Other models differ from each other on the sudden character of the transition. The latter is, of course, expected to be smooth in thermal as well as cold fragmentation models. It is more sudden in condensation and percolation models, where it exhibits features of a phase transition when the process is studied in variation of a parameter indicating the violence of the collision (excitation energy, temperature, impact parameter, or anything else).

It would be nice to check some of these conjectures or hypotheses in a dynamic model of the collision. The most sophisticated and still tractable one is the intranuclear cascade (INC) model. That is what we propose to do in this paper, adapting to this particular problem the cascade model that we successfully used for heavy ion reactions [15]) and for antiproton annihilation on nuclei [16]). Of course, the INC model carries a limited picture of the physics and its use can provide an answer on some of the above-mentioned aspects only. We will try to single out which of the

issues can be clarified and which cannot. Our general purpose is to analyze all the aspects of the energy transfer between the incident proton and the target in the 100 MeV–10 GeV range.

The paper is organized as follows. In sect. 2, we describe the INC model. In sect. 3, we present our results. We analyze the time evolution of the energy transfer, of the matter density and of the ejection of partciles from the target. We determine the energy, target mass, and impact parameter dependence of the energy loss. As a by-product of our calculation, we make a prediction of the nuclear stopping power in the energy range under consideration. Although extensive comparison with experiment is not the main purpose of this paper, we compare in sect. 4 our predictions with some measurements of Nakai's group. Sects. 5 and 6 deal with the fluctuations (from event to event) in the energy loss and in the number of ejected nucleons, respectively. In sect. 7, we try to distinguish between fast ejectiles and slow ejectiles supposed to come from evaporation. We tentatively relate the number of fast nucleons with the number of vacancies in percolation models. In sect. 8, we investigate the possible link between our model and the possible gas–liquid phase transition. Assuming the system is close enough to equilibrium for these considerations to be (at least partly) meaningful, we follow the trajectory of the system in the energy-entropy plane. Finally, sect. 9 contains our conclusion.

2. The intranuclear cascade model

2.1. THE MODEL

We have adapted to proton–nucleus collisions the INC model, primarily build for heavy ion collisions in the GeV range. The description of this model can be found in ref. [17]) and in references cited therein. In short, it depicts the process as a succession of binary collisions well separated in space and time. The particles move along straight lines until a pair of them reaches its minimum relative distance. If this is small enough, the particles can be deflected. The final momenta of the particles are determined at random in agreement with conservation laws and experimental cross sections. Inelasticity is taken into account by introducing the following reactions:

$$\mathrm{NN} \rightleftarrows \mathrm{N}\Delta\,, \qquad \Delta \rightleftarrows \pi\mathrm{N}\,. \tag{2.1}$$

The final channels are chosen at random in proportion of the total cross sections.

Several modifications have been introduced, as described below.

(i) The nucleons inside the target are assumed to move in a spherical constant potential well of depth V_0. When a nucleon hits the surface, it can either be reflected or escape from the target. The probability for transmission is taken as a relativistic generalization of the formula for a potential step

$$T = \frac{4p(p^2 - 2mV_0 + V_0^2)^{1/2}}{[p + (p^2 - 2mV_0 + V_0^2)^{1/2}]^2}, \tag{2.2}$$

where p is the incident momentum of the nucleon. In leaving the nucleus, the momentum is not conserved. Therefore, we do not expect a strict conservation of momentum but, as we will see, due to many compensating different motions, the lack of conservation is small on average. The energy is nonetheless conserved, provided the potential well is considered as a scalar field acting on the particles. Throughout this paper, V_0 is chosen as 40 MeV.

(ii) The treatment of delta's and pions has been improved in view of the energy range investigated here. First, the Δ production is not taken as isotropic anymore. In fact, the differential $NN \to N\Delta$ cross section is taken as

$$\frac{d\sigma}{d\Omega} \propto e^{B(s)t}, \tag{2.3a}$$

where t is the squared four-momentum transfer and where s is the squared c.m. energy. The function $B(s)$ is taken as for the elastic scattering [18]), which seems to be a reasonable choice [19]).

(iii) The π^+-p cross section (of which is derived the isospin averaged πN cross section) is taken as [20])

$$\sigma = \frac{\sigma_0}{1+4[(\sqrt{s}-E_0)/\Gamma]^2} \frac{q^3}{q^3+\mu^3}, \tag{2.3b}$$

where $\sqrt{s}$ is the c.m. energy and q the c.m. momentum. The numerical values are: $\sigma_0 = 326.5$ mb, $E_0 = 1215$ MeV, $\Gamma = 110$ MeV, $\mu = 180$ MeV/c.

(iv) In order to account for the π-absorption above the Δ-resonance (which once again cannot be neglected in view of the energies studied here), we assume that a Δ is formed (in πN system) whenever the total energy is below 3 GeV. Moreover, we used eq. (2.3b) up to $\sqrt{s} = 1.4$ GeV. Above that value, $\sigma(\pi^+ p)$ is taken equal to 50 mb, once again to account for the pion absorption.

2.2. CONSERVATION LAWS

It is useful for the analysis of the results to split energy, momentum and baryon number into different contributions. To simplify the notation, we write the equations non-relativistically, although relativistic kinematics has been used. Let us call W_p^0 the total energy of the incident proton, K_A^0 the kinetic energy of the nucleons inside the target at initial time. Let W_p and K_A be the values for the same quantities at later times. Let N_{ej} be the number of target nucleons which have left the potential well (the ejectiles), and A_{res} the remaining ones. If K_{ej} is the kinetic energy of the ejectiles and if W_π is the total energy carried by the pions, we can write ($c = 1$)

$$W_p^0 + (K_A^0 - AV_0) + AM = W_p + (K_{res} - A_{res}V_0) + A_{res}M + N_{ej}M + W_\pi + K_{ej}, \tag{2.4}$$

where A is the target mass number and where M is the nucleon mass. The parentheses stand for the target internal energy in our model. We have to emphasize that this

is indeed the energy in the extreme single-particle picture, which oversimplifies the interaction energy. The latter would be reduced by a factor 2 in the Hartree-Fock picture. Taking inside our model a value of V_0 of half the usual value is not a viable choice, wince then the nucleus will evaporate nucleons spontaneously, the Fermi energy being in such a case larger than the potential step. Therefore we choose $V_0 = 40$ MeV, overestimating the binding energy. But we have to remind that we are mainly interested in relative variations, for which the error will be much smaller. Concerning this point we may rewrite eq. (2.4) as

$$W_p^0 + (K_A^0 - AV_0) + AM = W_p + ((A_{res}/A)^{5/3} K_A^0 - A_{res} V_0) + E^* + A_{res} M + N_{ej} M + K_{ej} + W_\pi \quad (2.5)$$

with

$$E^* = K_{res} - (A_{res}/A)^{5/3} K_A \,. \quad (2.6)$$

The parentheses on the r.h.s. of eq. (2.5) can be considered as the smallest energy contained in a potential well enclosing a given number A_{res} of nucleons (the power $\frac{5}{3}$ comes from the Fermi-gas law). It can be regarded as the ground state energy of the residual nucleus in our simplified picture. This however neglects the modification of the average field and therefore can be true for residual nuclei close to the target nucleus only. Likewise E^* can be considered as the excitation energy. Clearly eq. (2.6) shows that, in the limited picture adopted here, the excitation comes from the ("thermal") excitation of the Fermi motion only.

Similarly to eq. (2.4), one can write the conservation law for the baryon number

$$A = N_{ej} + A_{res} \quad (2.7)$$

and for the momentum.

$$\boldsymbol{p}_0 + \boldsymbol{P}_A = \boldsymbol{P}_{res} + \boldsymbol{P}_{ej} + \boldsymbol{p} + \boldsymbol{P}_\pi \,, \quad (2.8)$$

where $\boldsymbol{p}_0$ is the incident momentum, $\boldsymbol{P}_A$ is the target momentum (due to Fermi motion in our picture), $\boldsymbol{P}_{res}$ is the momentum contained in the target volume, $\boldsymbol{P}_{ej}$ is the momentum of the ejectiles, $\boldsymbol{p}$ is the momentum of the incident proton and $\boldsymbol{p}_\pi$ is the momentum of the pions.

Of course eqs. (2.5), (2.7), (2.8) are valid event by event and for the average quantities as well. In particular, $\langle \boldsymbol{P}_A \rangle = 0$. A small remark has to be made for eq. (2.5). The conservation law for the average over the events indicated by the brackets writes

$$W_p^0 + (\langle K_A^0 \rangle - AV_0) + AM = \langle W_p \rangle + (\langle (A_{res}/A)^{5/3} K_A^0 \rangle - \langle A_{res} \rangle V_0) + \langle E^* \rangle + \langle A_{res} \rangle M + \langle N_{ej} \rangle M + \langle K_{ej} \rangle + \langle W_\pi \rangle \,. \quad (2.9)$$

Note that the first term in the parenthesis of the r.h.s. does not factorize into product of averages. In fact, we observed a rather strong anti-correlation between the two factors. It means that if K_A^0 is accidentally large, A_{res} is likely to be small and vice-versa (see below).

2.3. ENTROPY

Later, we will consider the creation of entropy during the collision process. Here, we just explain how the entropy is calculated. We record the positions and momenta of all the particles, for every run of the calculation. This amounts to generating the one-body distribution $f(\boldsymbol{r}, \boldsymbol{p}, t)$ for the nucleons. The entropy is defined by

$$S = -4 \int \frac{\mathrm{d}^3 r \, \mathrm{d}^3 p}{(2\pi\hbar)^3} [\tfrac{1}{4} f \ln \tfrac{1}{4} f + (1 - \tfrac{1}{4} f) \ln (1 - \tfrac{1}{4} f)] , \tag{2.10}$$

where we have assumed perfect spin–isospin degeneracy. We have replaced the six-dimensional integral by a three-dimensional integral, by assuming that the density in real space is spherical and that the density in momentum shows a cylindrical symmetry around the beam axis. In this case, a three-dimensional mesh is sufficient to sample the function f. In any case, we will make an estimate of the precision along the method described in ref. [21]).

3. Numerical results

3.1. TIME EVOLUTION

Fig. 1 gives in a typical example (central collisions of 1 GeV protons by ^{40}Ca nucleus) the time evolution of the quantities contained in eq. (2.7). Practically no particle is ejected before the incident proton has escaped from the nucleus. This moment is indicated approximately by the vertical arrow. Note that the number of participants, i.e. the particles which collide, is substantially larger than the number of ejectiles. This shows that some excitation is left in the nucleus.

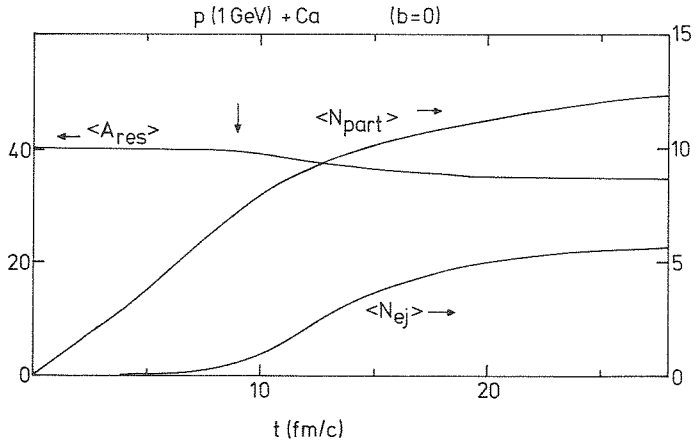

Fig. 1. INC calculation of time evolution of the target mass (A_{res}), of the number of ejected nucleons and of the number of participant nucleons in central collisions of 1 GeV protons with Ca nuclei.

This aspect is illustrated in fig. 2, which gives the time variation of the quantities entering in the energy conservation law, eq. (2.9). It is remarkable that at $t \simeq 9$ fm/c, when the incoming proton reaches its asymptotic energy, the excitation energy of the nucleus is around its maximum and practically no energy has been carried away by the ejectiles. It is a bit surprising that the excitation energy is evacuated on so short a time scale. But, at the beginning, the targets emit fast nucleons. Only after some time (~25 fm/c), the ejected nucleons have a kinetic energy of ~20 MeV, and the emission is then akin to ordinary evaporation. This stage seems to correspond to a longer time scale.

Fig. 2 also displays the entropy contained in the nuclear volume. This entropy decreases because of the flow of entropy carried by the ejectiles.

The characteristic time evolution of the various quantities remains the same at higher energies. The deposition of energy is rather well separated from the ejection of the nucleons. Of course the amount of energy deposit is not the same (see later on). At low energy, the two stages of the process are less well separated. Actually, the energy deposit is rather small.

3.2. DENSITY PROFILES

In fig. 3, we display the baryon density in the reaction plane for central collisions of 2 GeV protons on Ca nuclei. The incident proton is not included in these plots.

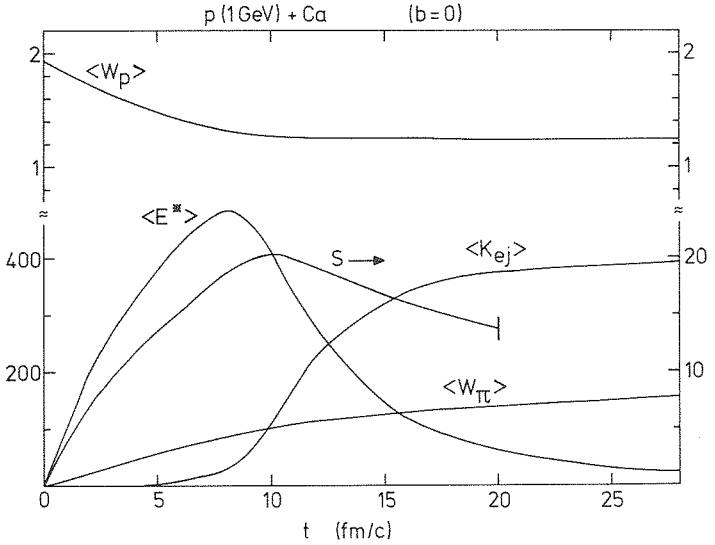

Fig. 2. INC calculation of the time evolution of the various quantities entering into the conservation law (eq. (2.9)) for central collisions of 1 GeV protons on Ca nuclei. The upper curve gives the total energy of the incident proton. The quantity E^* is the excitation energy of the residual nucleus. The quantity K_{ej} is the kinetic energy of the ejected nucleons and W_π is the total energy of the pions. Finally, S is the entropy of the residual nucleus.

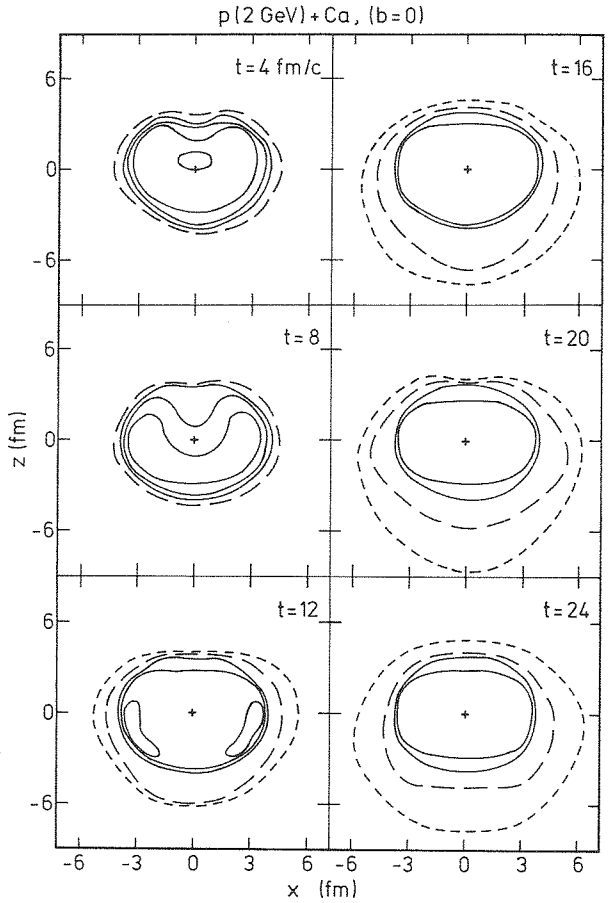

Fig. 3. Density profiles in the reaction plane for central collisions of 1 GeV proton with ^{40}Ca. At $t=0$ the proton, coming from above, is supposed to hit the surface. The curves are isodensity curves. The full curves represent $\frac{1}{3}$, $\frac{2}{3}$, 1, $\frac{4}{3}$ times ρ_0, respectively, starting from outside ($\rho_0 = 0.17$ fm^{-3} is the normal nuclear matter density). The long dashed curve and the dotted curve correspond to $\frac{1}{30}$ and $\frac{1}{60}$ of ρ_0, respectively. See text for more detail. Note the different scales in the x- and z-directions.

These figures are obtained by counting the baryons in cells (roughly cubes of 1.2 fm side) for a thousand runs. The isodensity curves are obtained by interpolation between the values at the mesh points. This procedure smooths the nuclear surface. The lack of complete right-left symmetry is due to the statistics. In these plots, the original nucleus appears deformed, because the plotting routine uses different scales in the two directions.

In the very early stage, the incident proton compresses a little bit the matter ahead (the maximum density observed is about 1.3 times ρ_0). Also it leaves a conical depression behind. This conical pattern evolves up to 12 fm/c. Afterwards the density inside the nuclear volume tends to become uniform. At the same time, particles are emitted outside. Actually, there are particles emitted well beyond the outermost

dotted curve in fig. 3. The density of the residual nucleus is smaller than the normal density, because of nuclear depletion.

3.3. ENERGY DEPENDENCE

We have looked to the energy dependence of the various (asymptotic) quantities entering in the conservation laws written down in sect. 2. The most interesting one is probably the energy loss

$$\Delta E = W_p^0 - \langle W_p \rangle \tag{3.1}$$

of the incident proton. It is shown in fig. 4 for central p-Ca collisions and in fig. 5 for central p-Au collisions. In both cases, the energy loss increases until 10 GeV incident energy and decreases for larger energy. Within our model, this decrease is due to the decrease of the total NN cross section (whose parametrization, primarily designed for the 1-4 GeV range, underestimates by 10-20% the value around 20 GeV), to the strongly forward-peaked NN elastic scattering and to the excitation of only one resonance, namely the Δ-resonance, in the inelastic scattering. The total inelastic cross section is close to the experimental one (in pp channel at least), but the excitation of heavier resonances, although starting slowly, becomes important in the 10-20 GeV range. Therefore, the calculation at 20 GeV is certainly not reliable. We expect rather a saturation of the energy loss above 10 GeV.

In the 1-10 GeV range, the energy loss obeys more or less the following law

$$\Delta E = 0.75 + a \ln E_{\text{inc}}, \tag{3.2}$$

with $a = 0.63$ for ^{40}Ca and $a = 1.32$ for ^{197}Au, where everything is expressed in GeV.

A part of the energy loss is used to create pions. The rest is transferred to the nucleon system. It is shown (by the crosses) in figs. 4 and 5. This quantity seems

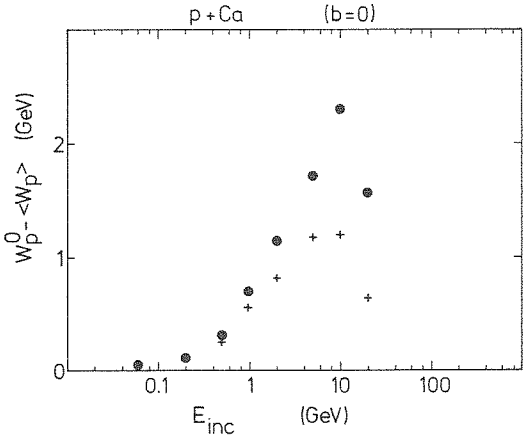

Fig. 4. Energy loss in central collisions of protons with ^{40}Ca nuclei. The dots correspond to the total energy loss, and the crosses to the part of this quantity which is not used to create pions.

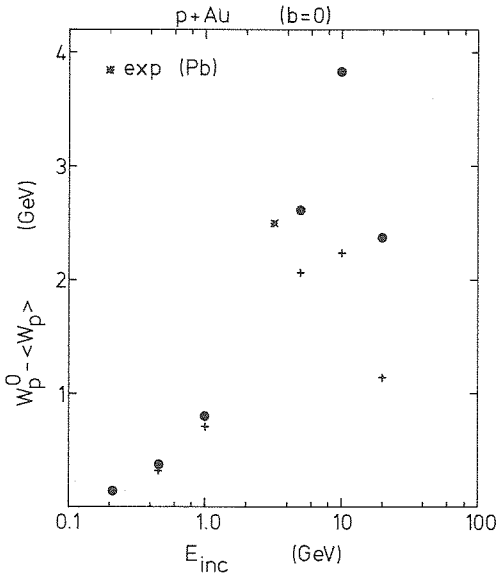

Fig. 5. Same as fig. 4 for central collisions on Au nuclei. The experimental point comes from ref. [25]). See sect. 4 for some detail.

to saturate earlier than ΔE, i.e. around ~5 GeV. The saturation value is ~1.2 GeV for Ca nuclei and ~2.2 GeV for Au. In other words, above 5 GeV, the extra energy loss is primarily expanded into the production of pions.

It is interesting to know that fraction of the available energy the energy loss represents. This is actually contained in fig. 6 (by the crosses, see discussion later on for the dots). This fraction shows a maximum around 1 GeV. This is mainly due to the more and more forward-peaked elastic cross section, which makes the latter process less and less efficient for the energy transfer.

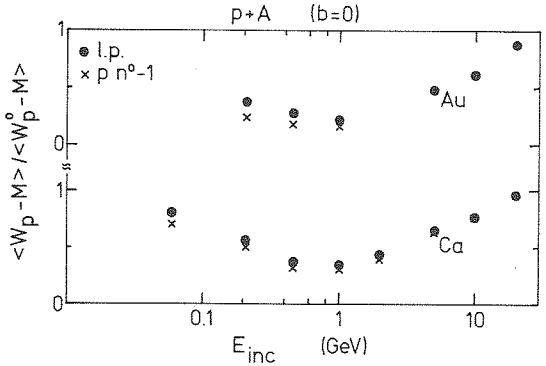

Fig. 6. The crosses represent the ratio of the final energy of the incident proton by the available energy for central collisions of protons with Ca and Au nuclei. The meaning of the dots is explained in sect. 5.

In figs. 7 and 8, we display the energy dependence of the number of ejectiles, of the number of produced pions and of the number of participants. A remark has to be made concerning the meaning of these quantities. As fig. 2 indicates the final value of these quantities is fixed at very late times. In order to give a precise value, the cascade should be run for a very long time. In general, we stopped the cascade when the emission of soft nucleons sets in. There is however no well-defined beginning of this stage. For instance, observation of fig. 2 reveals that even after the excitation energy has got down to ~1 MeV per nucleon, there is still a substantial

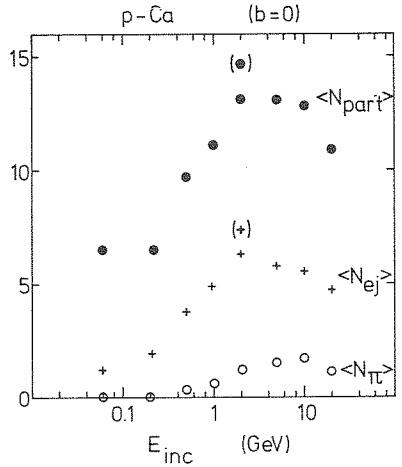

Fig. 7. Energy dependence of the average number of participants, the average number of ejectiles and the average number of pions, respectively, for central collisions on Ca nuclei. The meaning of the symbols in parentheses is discussed in the text.

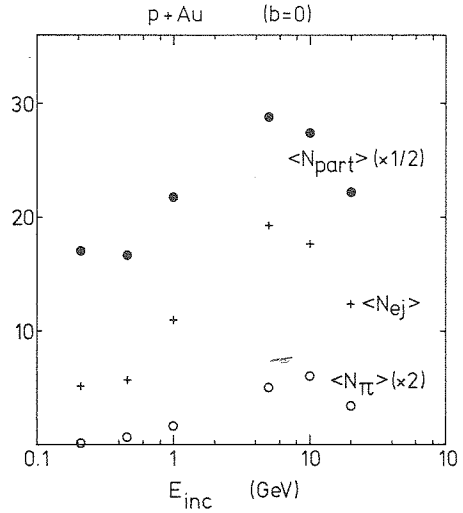

Fig. 8. Same as fig. 7 for Au targets.

emission of (of course slow) ejectiles. As a matter of fact, the nucleons are still colliding (with a decreasing rate) within the nucleus, increasing probably for a long time the number of participants and consequently, the number of ejectiles. Figs. 6 and 7 give the values of the quantities at the beginning of the soft process, i.e. around $t \sim 20$ fm/c for Ca and $t \sim 30$ fm/c for Au.

For the particular case of 2 GeV protons on Ca, we also indicate the values at a later time, namely 30 fm/c. The number of pions does not change significantly, whereas the number of ejectiles still increases by about 20%. It can be seen also that the number of ejectiles increases to about 5 GeV and decreases further on.

Of course, the soft evaporation process is the least suited to be described by the cascade model, because the Pauli principle is expected to be sensitive to details of the wave functions and more importantly because the evaporation is likely influenced by complicated configurations and not simply by the single-particle motion. In other words, we believe the INC model is not reliable for the late soft evaporation stage.

3.4. MASS DEPENDENCE

This aspect has partly been discussed in the previous subsection. Obviously, the energy loss increases with the mass of system. This is mainly a geometrical effect, as the number of interactions increases with the mass of the target. The mass dependence is summarized in fig. 9. The number of ejectiles as well as the number of particles roughly follows a $A^{1/3}$ law. For the energy loss the geometrical dependence seems to be more involved.

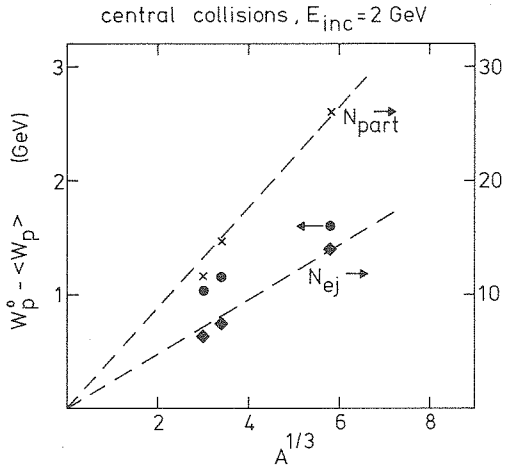

Fig. 9. Target mass dependence of the energy loss (dots), of the number of participants (crosses) and of the number of ejectiles (lozenges) for contral collisions of 2 GeV protons. The straight lines indicate the approximate $A^{1/3}$ law.

3.5. IMPACT PARAMETER DEPENDENCE

As for the mass dependence, the impact parameter b introduces another geometrical effect. The variation of the energy loss with the impact parameter b is shown in fig. 10 (lower part) for a typical example. The upper part of the figure describes the b-dependence of the number of ejectiles (the number of participants, not shown, falls on the same curve). Except for the large impact parameters, the

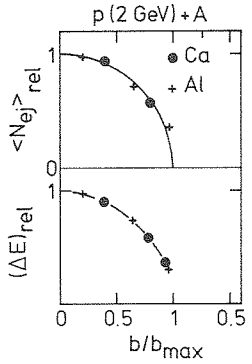

Fig. 10. Impact parameter (b) dependence of the relative energy loss (lower part) and of the relative number of ejectiles (upper part), i.e. normalized to their respective values at zero impact parameter, for collisions of 2 GeV protons with Ca and Al targets. The line in the upper part represents a semi-circle law. The line in the lower part is just to guide the eye.

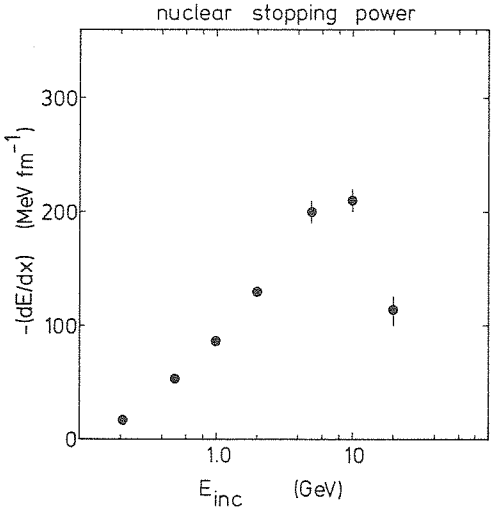

Fig. 11. Nuclear stopping power as predicted by our model. Values are obtained by averaging over Ca, Al and Au targets and on several impact parameters (less than 0.8 times the maximum values). The dispersion on the various conditions are indicated by the error bars, when the latter are larger than the width of the dots.

variation of $\langle N_{ej} \rangle$ follows a semi-circle law, i.e. that the $\langle N_{ej} \rangle$ is proportional to the length that the incident proton would travel inside the nucleus if its motion was along a straight line (see later). The b-dependence is very similar for the energy loss.

3.6. NUCLEAR STOPPING POWER

We can determine this quantity by looking at the space-variation of the incident proton energy when it enters the nucleus. The specific energy loss is not dependent (less than 5%) upon the target and upon the impact parameter. Therefore the nuclear stopping power seems a well-defined quantity at least in our model. Its dependence upon the proton energy is depicted in fig. 11. In agreement with the preceding results, it increases up to 10 GeV incident energy. Once again, the point at 20 GeV is to be taken with caution, since the stopping power is more likely to saturate rather than decrease.

4. Comparison with experiment

The extensive comparison of the model predictions with experiment is delayed to a forthcoming paper. We want here to concentrate on the main features of the model and on its relationship with fragmentation models. However, we want to show here on one case that the model provides a reasonable first approach to proton-nucleus interactions in the 1 GeV-a few GeV range. Surprisingly, energy loss and particle production measurements are very scarce in this energy range. We have particularly paid attention here to those of Nakai's group [22-24]). We have investigated the two main aspects of the dynamics, namely the slowing down of the incident proton and the ejection of the particles at large angles.

The first of these features can be characterized by the so-called stopping cross section [24]). In this reference, it is defined as the cross section for having no particle in the detector in the forward direction. Although very convenient, this definition presents the disadvantage of being specific to a given apparatus. As a consequence, this makes comparison with theoretical models difficult, since the acceptance of the apparatus is not always easy to simulate, due to the presence of neutral particles and also the production of composites, which are not always accounted for in theoretical models (it is not in ours, of course). Therefore, we present in fig. 12 a tentative comparison with the experimental data. In our calculation, the stopping cross section is defined as the cross section for having no nucleon of more than 25 MeV lab. energy at angles less than 10°, as in ref. [24]). The predicted ratio of stopping to geometrical cross sections ($r_0 = 1.12$ fm) does not depend very much upon the target size. It drops by 20-25% when going from Al to Au, which in the scale of fig. 12 is within the errors of the calculation. The latter include not only statistics, but also uncertainty on the description of the acceptance of the detector.

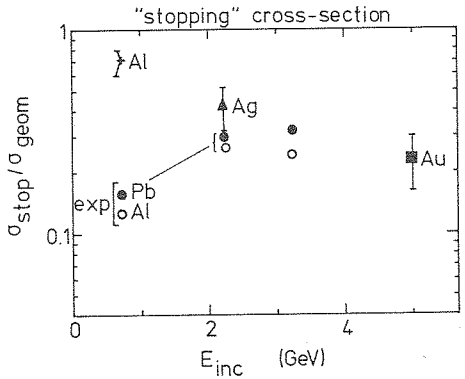

Fig. 12. Ratio of the stopping cross section to the geometrical cross section as a function of the proton incident energy. The experimental data are taken from ref. [22]) are indicated by the dots. The other symbols correspond to the results of our calculation whose typical uncertainty is given by the error bars. See text for detail.

We reach a reasonable agreement, although the calculations seem to overestimate the stopping cross section in the 2–3 GeV range*.

Concerning the energy loss itself, we have reported, in fig. 5, the proton energy loss in high multiplicity events (which can be considered as corresponding to central collisions) induced by 4 GeV/c incident protons on Pb nuclei. As can be seen, our predictions for Au compare quite well to this measurement. However, the author of ref. [25]) observed a surprisingly much larger energy loss in the case of the Al target, a feature which is certainly not consistent with our predictions.

In ref. [22]), it is observed that the experimental inclusive proton cross section at 90° lab. presents an exponential fall-off with the energy:

$$E\frac{d^3\sigma}{dp^3} \propto \exp(-E/E_0)\,. \tag{4.1}$$

The slope parameter E_0 is shown in fig. 13 along with the predictions of our model. Here also the results do not significantly depend upon the target size. The model turns out to provide a reasonable agreement with the data, although the predicted value around 1 GeV is clearly too small.

5. The energy loss and the fluctuations

5.1. THE INCIDENT PROTON

In the present INC calculation, we keep track of the incident proton. From the practical point of view, this is done as follows. We give to the incident proton the tag no. 1. Whenever particle no. 1 makes a collision, the particle with the largest

* It now seems [unpublished ref. [25]), cited in ref. [26])] that a new analysis of the experiment leads to increased stopping cross sections. If this turns out to be the case, our model would rather underestimate the stopping cross sections.

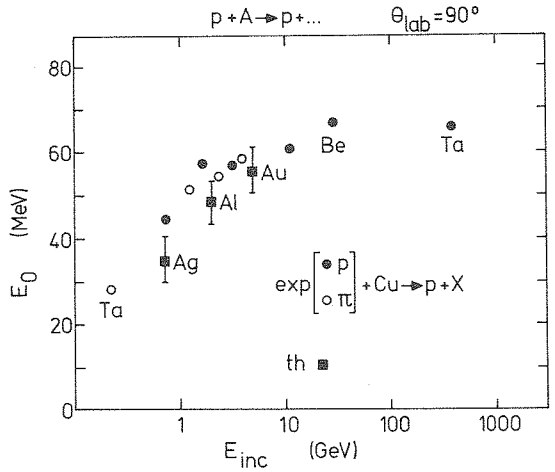

Fig. 13. Parameter E_0 characterizing the energy spectrum of the protons emitted at 90° lab. (see eq. (4.1)), as a function of the proton incident energy. The experimental data [22]) are indicated by the dots. The squares correspond to the results of our calculation. Typical uncertainty of the latter is given by the error bars. See text for detail.

longitudinal velocity receives the tag no. 1. In this way, it is possible to follow the fate of the incident proton and to speak about the time evolution of its properties. However, in an actual measurement, the object of interest is the leading particle, i.e. the particle with, say, the largest velocity. Whether this particle is the incident proton or not is irrelevant in view of the fermion statistics. However, in a particular model like ours, one can inquire whether in fact the leading particle is particle with tag no. 1 or not. It is easy to realize that this is *not* guaranteed by the procedure described above. At high energy ($\geqslant$1 GeV), where the transverse motion is limited, this is almost always the case. At low energy the probability that this is not so can be substantially large. This, for instance, is reflected by fig. 6, where the final energy refers to either the leading particle (dots) or the particle no. 1, the "incident proton". Everywhere else in this paper, the quantities referred to concern the incident proton.

5.2. PRIMARY COLLISIONS

One of the important features of the dynamics is the number of collisions suffered by the incident proton, referred to as the primary collisions. The average number is given in table 1 for central collisions on Ca and Au nuclei. We have checked that, for a given energy, the number of collisions is roughly proportional to the length that the projectile would travel inside the target if it propagates along a straight line. The number of collisions is less than what would be expected by dividing the length of this path by the classical mean free path (evaluated with the cross section at the incident energy). There are three causes responsible for this effect. First, the incident proton slows down, and the effective cross section is reduced

TABLE 1

Average number $\langle n \rangle$ of primary collisions ($b = 0$)

				p+Ca			
E_{inc} (GeV)	0.06	0.21	0.5	1.0	2.0	5.0	10
$\langle n \rangle$	1.01	1.65	2.19	2.87	3.93	4.14	3.39
$\langle n \rangle$ (no PB)					4.11		
				p+Au			
E_{inc} (GeV)	-	0.21	0.5	1.0	-	5.0	10
$\langle n \rangle$	-	1.91	2.36	2.85	-	6.66	5.93

The average number n of primary collisions is given as a function of the incident energy for central collisions. The line labelled "no PB" corresponds to the removal of the Pauli blocking.

compared to the "high energy" 40 mb. Second, the Pauli principle inhibits some primary collisions. This effect is small but not negligible, even at high energy. In table 1 we indicate that it is about 5%. This effect is not reduced when going towards higher energy, because the average momentum transfer to the target nucleon is comparable to the Fermi momentum and, therefore, the collision can be blocked. The third cause is more subtle. At high energy, each primary collision has about 50% chance to transform the incident proton into a Δ-resonance and the latter propagates with a smaller total cross section (for detail, see sect. 2 of ref. [27])).

Fig. 14 gives the fluctuations in the number n of the primary collision. It is interesting to note that the fluctuations are typical of a Poisson law, a property

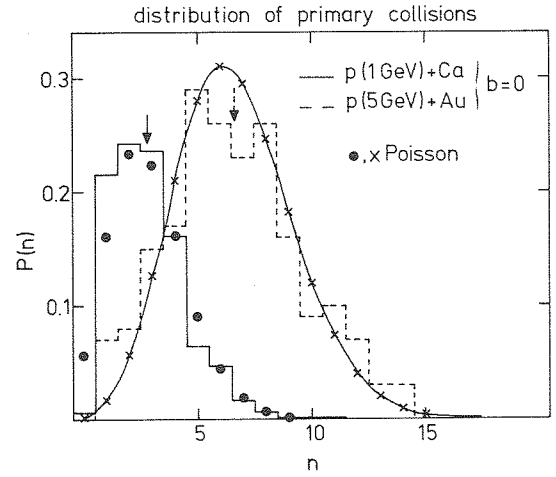

Fig. 14. Probability distribution for the number n of primary collisions (histograms) as calculated in the INC model for the two cases indicated in the upper right corner. The dots and the crosses are Poisson distributions with the same mean as the two histograms, respectively. The mean value of n is indicated by the vertical arrows.

which is repeatedly assumed in the literature, especially in the context of Glauber approach. But, to our knowledge, this was never tested in a realistic multiple scattering model.

5.3. THE ENERGY LOSS

Fig. 15 shows another aspect of the fluctuations, namely those arising in the energy loss. There is a striking difference between the situation at 1 GeV and the situation at 5 GeV. In the former case, the distributions shows a sharp edge close to the maximum energy loss and a smooth tail extending up to much smaller energy loss. At 5 GeV the proton can also lose all the available energy, but the distribution is much broader. This seems to result from the larger number of collisions and from two opposite effects: the creation of Δ-resonances, which favours the energy loss and the strongly peaked elastic angular distribution, which tends to reduce this quantity.

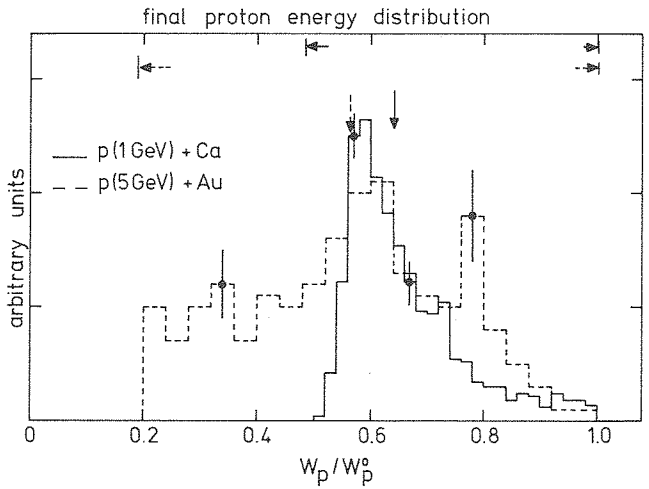

Fig. 15. Distribution of the final proton (total) energy W_p for central collisions in the two cases indicated on the left. The quantity W_p^0 is the incident proton energy. The vertical arrows indicate the average value. The horizontal arrows delineate the accessible range for the ratio W_p / W_p^0 in the two respective cases. The error bars indicate the uncertainty of the calculation.

Another basic quantity is the energy loss per primary collision. We show the average (over events) of this quantity in fig. 16. This quantity increases rather fast with the incident energy. This situation reflects the overwhelming importance of the resonance excitation. The elastic scattering alone would give less than 200 MeV above 2 GeV incident energy. This can be estimated from the differential elastic cross section [18]). Yet the increase of the energy loss per primary collision is not sufficient to destroy the forward motion of the incident proton. On the contrary the

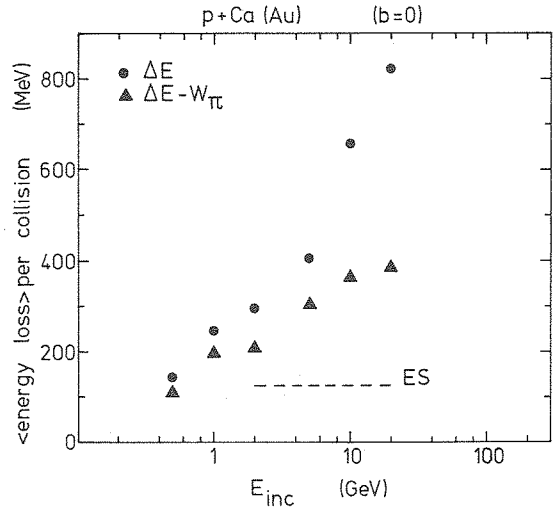

Fig. 16. Average energy loss (dots) per primary collision for central collisions on Ca and Au targets. The dots indicate the average over the two targets, but the differences are a few percent at most. The triangles are obtained after removal of the part of the energy loss used to create pions. The dotted line indicates the estimate of what would be the energy loss due to elastic scattering alone (at the incident energy). See text for details.

higher the energy, the less the proton is deviated as indicated in fig. 17. Of course, this is due to the large longitudinal momentum compared to the acquired perpendicular momentum. It is remarkable, however, that the inelastic scattering does not increase $\langle p_\perp \rangle$ very much here. If a single elastic scattering occurs, the estimated $\langle p_\perp \rangle$ would be ~360 MeV/c above 2 GeV incident energy. This is indicated by the dotted line in fig. 17.

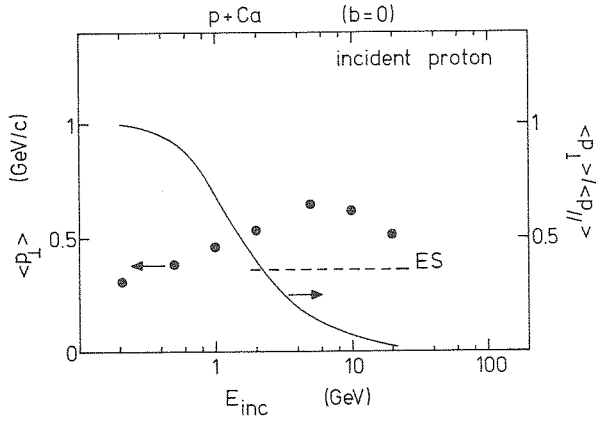

Fig. 17. Average final perpendicular momentum (dots) of the incident proton as a function of its initial energy in central collisions on ^{40}Ca nuclei. The full line (scale on right) indicates the ratio of the final average perpendicular to average longitudinal momentum. The dotted line indicates the value of $\langle p_\perp \rangle$ caused by a single elastic scattering.

Let us make a few remarks here. First, the bouncing of the nucleons on the potential wall induces, as we said, a lack of absolute momentum conservation. But if we consider the whole nucleus, we check that this violation never exceeds more than 20 MeV/c in the GeV range. This should be compared with the incident momentum, which is at least 80 times larger.

In the course of the reaction mechanism, the momentum gained by all the nucleons inside the target can be quite large. To fix the ideas, it can be of the order of 1 GeV/c (mainly in the forward direction) for 3 GeV/c incident proton. This would probably induce an important recoil of the nucleus triggered by the nucleons bouncing on the wall. This would not however change very much the number of ejectiles, since the excitation energy will be negligibly modified by the recoil.

Finally, for intermediate impact parameter, we noticed that the proton can be preferentially deflected away from the target. But the quantitative importance of this effect is very small. At 2 GeV, the average value of $\langle p_x \rangle$ (along the impact parameter axis) is of the order of 30 MeV/c only.

6. The ejectiles

6.1. ENERGY SPECTRUM

The ejected nucleons have a very broad energy spectrum as can be seen in figs. 18 and 19. The low energy part of the spectrum ($\lesssim$400 MeV) shows an exponential

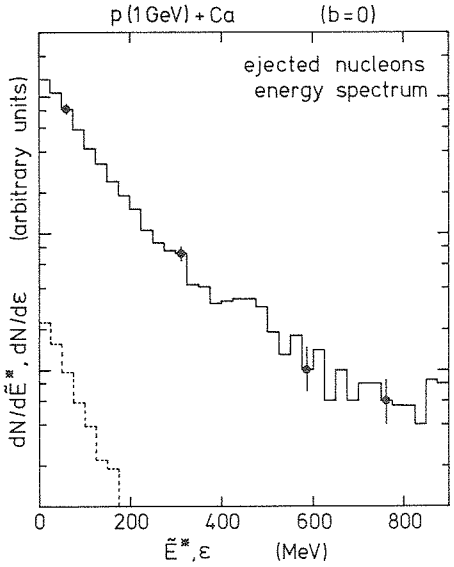

Fig. 18. INC calculation of central collisions of 1 GeV proton with Ca nuclei. Full line: kinetic energy (ε) spectrum of the ejected nucleons. Dotted line: distribution of the target excitation ($\tilde{E}^*$) at roughly the beginning of the soft evaporation process. The scale is arbitrary, but logarithmic. See text for details. The error bars are indicating the typical uncertainty of the calculation.

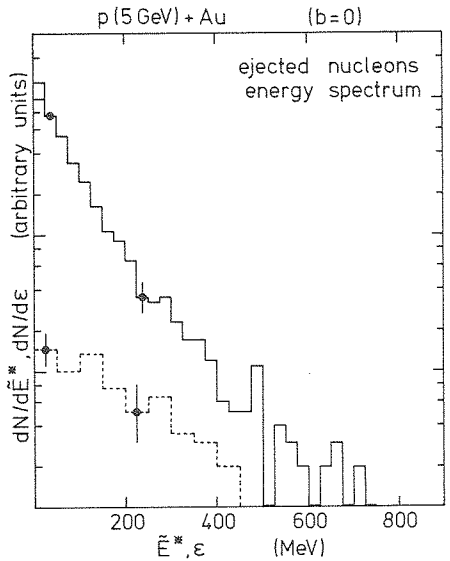

Fig. 19. Same as fig. 18 for 5 GeV protons on Au nuclei.

fall-off. It is however not realistic to consider this feature as indicative of a thermal emission, since many nucleons are ejected after making one or two collisions only. Moreover, as we will see later on and as can be guessed from fig. 2, the nucleons are emitted from a nucleus with many possible values of excitation energy, depending upon the emission time. A surprising result is that there are comparatively more high energy ejectiles in the case of 1 GeV protons on Ca compared to the one of 5 GeV protons on Au. A glance at fig. 16 makes us believe that this is essentially a geometrical effect. The energy transferred to the nucleons is not very different in both cases but a high energy nucleon can escape more easily from a Ca nucleus.

Figs. 18 and 19 give (dotted lines) the dispersion in the residual nucleus excitation energy at the time of the beginning of the very slow evaporation process (see sect. 3.3). There seems to be a drastic difference between the two cases under consideration. In our opinion, this is linked to the fluctuations in the original energy deposition, or, equivalently, to the energy loss (see fig. 15).

6.2. NUMBER OF EJECTILES

There are substantial fluctuations in the number of ejectiles. These are depicted in figs. 20 and 21. In absolute values, the number of ejectiles is larger in Au compared to Ca. Yet, the proportion of ejected nucleons is larger in Ca. The ratio of the number of ejectiles N_{ej} to the target mass number barely exceeds 0.25 in the case of Au at 5 GeV (this increases with energy in this energy range, see fig. 7). For Ca targets, this ratio can go up to 0.5. Of course, it decreases with the impact parameter.

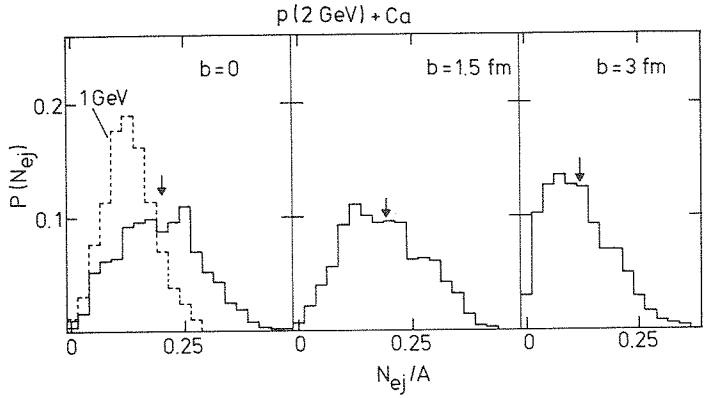

Fig. 20. Full curves: probability distribution for the number of ejectiles N_{ej} in the case of 2 GeV protons on ^{40}Ca. (A is the mass number of the target). The vertical arrows indicate the mean values. Dotted curve: same quantity for central collisions of 1 GeV protons on the same target.

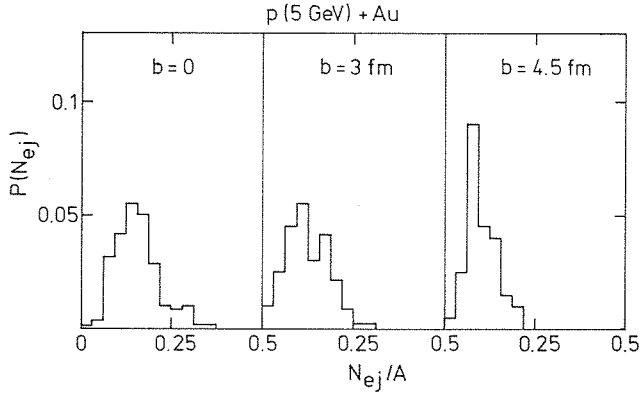

Fig. 21. Probability distribution for the number of ejectiles N_{ej} in the case of 5 GeV protons bombarding a ^{197}Au-target.

7. Fast ejectiles and percolation models

7.1. GENERALITIES

In the current percolation models for multifragmentation, it is generally assumed [12,13]) that the collision mechanism is composed of a rapid stage where a few highly energetic particles are ejected and a slow stage where the remnant fragments into several pieces. The extreme (and basic) idea in percolation is to state that the fragmentation pattern is solely determined by the number of fast ejectiles. If this number is large enough, the nucleus is expected to fragment in many pieces of comparable size just as in site percolation on a lattice. If not, the nucleus still evaporates a few particles, leaving behind a heavy fragment.

A connection can be made between our results and percolation models: we can predict the number of fast particles. What is a fast particle is not precisely defined. Studies at high energy have been made with emulsions [28-32]). A fast particle is there considered as a "grey" particle, i.e. a particle with low ionisation. Here, for simplicity, we arbitrarily define a fast particle (for convenience, we will call it grey also) as an ejectile having at least 20 MeV asymptotic energy. It is not obvious that we should not use a less rigid criterion. We, however, will indicate how our conclusions can be affected by this choice.

7.2. PROPERTIES OF THE FAST PARTICLES

One of the our results is contained in fig. 22. The histogram shows that the first emitted particles are much more energetic than the latest ones. There is no real indication of two regimes of emission. As a matter of fact, our model is expected to show a continuum of emission patterns. In this context it is somewhat arbitrary to distinguish between fast and slow particles. However, it can be considered that the single-particle motion of a fast particle is rather well described by our model. On the contrary the motion of a slow particle is expected to be very much distributed by what is missing in our model, namely coupling to more complicated configurations, correlations and so on. It is well-known that these effects are important in usual evaporation from compound nucleus [33]), i.e. for nucleons whose energy is less or of the order of 10 MeV. In conclusion, it may not be so arbitrary to make a separation around 20 MeV, isolating so the contribution for which an INC description is rather realistic.

The crucial quantity for the connection with the percolation models is the number of the fast or grey particles. In fig. 23, this quantity (averaged over events) is given as a function of the average number of primary collisions. It turns out that in the

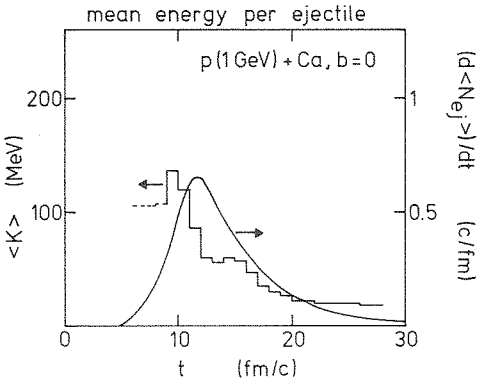

Fig. 22. Collisions of 1 GeV protons on Ca nuclei. Histogram: mean kinetic energy per ejectile as a function of the emission time (scale on the left). Curve: ejectile emission rate as a function of time (scale on the right).

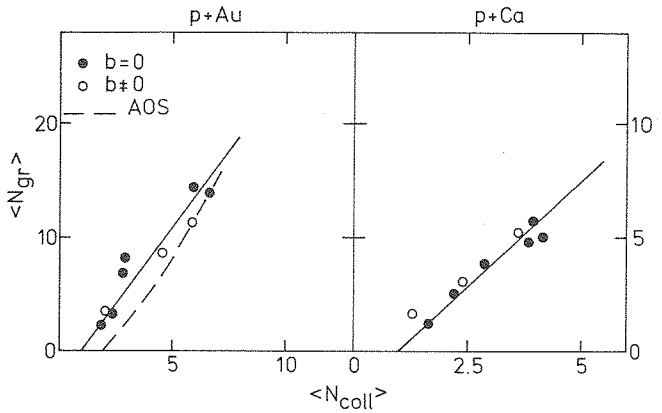

Fig. 23. Relationship between the average (over events) number of grey particles and the average number of primary collisions of the incident proton on Au targets (left part, scale on the left) and on Ca targets (right part, scale on the right). The black dots refer for central collisions for energies ranging from 250 MeV to 20 GeV. The open dots correspond to mid values of the impact parameter. The dashed line represents the relationship as extracted in ref. [34]) from high energy protons on the Ag or Br nuclei of an emulsion.

1-10 GeV range, for central as well as peripheral collisions, this relation is linear. It is interesting to note that this relationship is very close to the one existing at higher energies. The long dashes in fig. 23 indicate this relationship as extracted by Andersson *et al.* [34]), from 200 GeV interactions with emulsion. Actually, this curve refers to the heavy elements (Ag, Br). This agreement could be accidental as the collision regimes are probably different. At these energies a large part of the energy loss is used for producing pions (the so-called shower particles), whereas in our case, this part reaches 50% at the most.

The linear relationship can be expressed by

$$\langle N_{\mathrm{gr}}\rangle = a(\langle N_{\mathrm{coll}}\rangle - 1)\,, \tag{7.1}$$

with $a \simeq 2.7$ for Au and 1.85 for Ca.

7.3. LINK WITH PERCOLATION MODELS

If the number of *grey* particles is taken as the number of removed sites in a percolation model and if we express by p the number of remaining sites compared to the original one, fig. 23 indicates that $\langle p\rangle$ is never small. At least $\langle p\rangle \simeq 0.93$ for Au and $\langle p\rangle \simeq 0.88$ for Ca. This is well above the critical value in the percolation model of ref. [13]) ($p_c \simeq 0.55$) and even of lattice percolation in two dimensions [35]) ($p_c \simeq 0.60$). However, a recent analysis [36]) of exclusive measurements [37]) (in heavy ion reactions, however) would indicate that, *if a percolation picture is appropriate to the nuclear case*, the critical concentration would be much larger ($p_c \simeq 0.85$). Incidentally, this would probably mean that in reality the percolation pattern would be

very different from the usual site percolation on a lattice. This could be an indication that other features than geometrical ones have to be taken into account. Still the average values of $\langle p \rangle$, suggested by our calculation, is over this "empirical" value of p_c. But, the fluctuations in p in our model are similar to those for the quantity N_{ej} (see figs. 20 and 21). Therefore, it is expected that in a limited number of events ($\sim$10–20%) the value of p becomes lower than $p_c \simeq 0.85$. For these events, the characteristic multifragmentation, i.e. the partition of the system in many fragments of equal size, is very likely. Further investigations along these lines, i.e. a scenario based on a microscopic model for the fast processes and on the percolation ideas for the latest slow processes, are certainly promising. However, the final relationship between p and N_{ej} is still under debate [51]).

8. Entropy and the liquid–gas phase transition

It has been suggested that the fragmentation of a target following a proton interaction (or in the course of heavy ion reaction) can be a manifestation of a liquid–gas phase transition involving the bulk matter. What would be the dynamical path of this matter is not clear at all. Even more, this phase transition can be masked by several aspects of nuclear systems, the most important of which are named Coulomb force, finite size and surface effect. These aspects can be incorporated in a chemical equilibrium model. But it is not clear whether the most important aspects are preserved. It seems nevertheless that the gross properties of the mass yield are very much akin to those expected from a bulk matter phase transition [9–10,38,39]), with however a considerable modification of the transition point.

The ideas about phase transition can be applied to equilibrated (or not far from equilibrium) systems. In a proton-induced reaction at high energy, the target experiences rapid changes (as we saw) which put it away from equilibrium. In our calculation, the target is never at equilibrium, since it keeps evaporating nucleons for a long time. However, one can reasonably admit that the equilibration process is slightly more rapid than indicated by our calculation. Features of the dynamics, neglected here, like multi-nucleon interactions, configuration mixing and so on, are certainly helping in that direction, especially at late times. But, for a while, we will consider that the target can be described thermodynamically by extensive variables and that the departure from equilibrium is not important, which seems an acceptable first approach. Then, the evolution of this system in the space of the thermodynamic variables proceeds from the energy-momentum transfer in the fast process. This point of view is the one adopted in refs. [40,41]), where the cascade is considered as a realistic tool to determine the time evolution of the (average) internal energy (E^* in our model) per nucleon and of the entropy per nucleon due to the energy deposit produced by the primary collisions and the evacuation of the very fast particles. What happens to an equilibrated system following a dynamical path in the $(E^*/A, S/A)$ plane is still a matter of discussion [38–47]). But, in any case, it is important

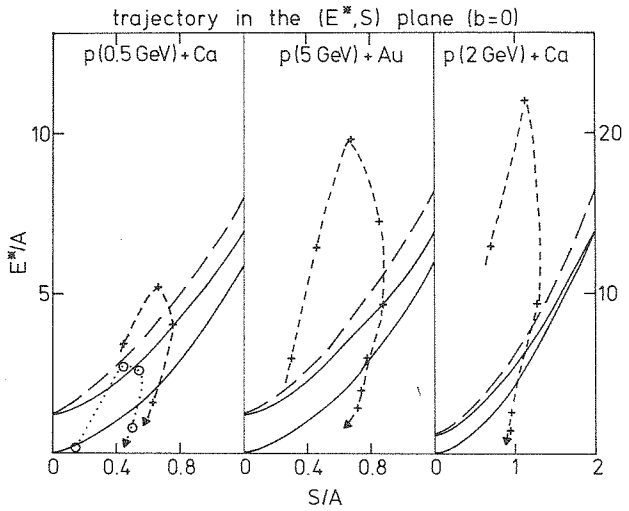

Fig. 24. Trajectory (short dashes) of the representative point of the target system in the internal (energy per particle, entropy per particle) plane, for central collisions of protons with nuclei. The crossses give the position of the representative point every 4 fm/c after the beginning of the collision. In each case, the lower full curve is the boundary of the coexistence zone, the upper full curve is the isothermal spinodal and the long dashed curve is the isoentropic spinodal. For the first case (left part), the representative point for a non central collision ($b = 3$ fm) is also shown by the circles.

to know whether the representative point of the system really enters the coexistence zone or the instability zone and if it does, for how long a time.

We summarize the most interesting cases we studied in fig. 24. In each part of the figure are reported the interesting branch of the coexistence curve, of the isothermal spinodal and of the isoentropic spinodal, respectively, as calculated from a Hartree-Fock calculation with the Skyrme III force*. In the lower right corner, the matter is liquid. Above the coexistence curve (the lowest of the full curves), the two phases (liquid and gas) can coexist. Above the spinodals, the matter is unstable (which one is relevant depends upon the possible transformation of the system).

For the central collisions in all the systems quoted, the representative point makes an excursion for a relatively long time ($\approx$16 fm/c or over) in the coexistence zone. Even if one disregards the first stage ($\sim$10 fm/c) dominated by the violent processes linked with the primary collisions, the time spent in this zone is still of the order of about 8 fm/c, which is a non-negligible time. Whether it is sufficient to permit a separation of the phase is poorly known (see ref. [48])). Except for the p (500 MeV) + Ca case, the representative point moves for a relatively long time in the instability zone. Once again, it is not at all sure that this time is long enough to induce fragmentation of the system by the onset of the instability.

The method, described in sect. 2, to calculate the entropy introduces some numerical errors, which, as explained in ref. [21]), generally overestimates the entropy.

* The results are not really sensitive to the effective interaction.

For the first part of the collision process, i.e. for times smaller than, say, 15 fm/c, the error is generally small, of the order of 0.1 unit or smaller. For later times, when the distribution in momentum space is close to a Fermi distribution with a small temperature, the numerical procedure is becoming worse. The latest points in fig. 24 can be given a numerical error of about 0.2 unit of entropy.

Our results are very much similar to those of Boal and Goodman [40]), who also used a cascade model. The two cascade models cover essentially the same dynamics. Ours is more realistic on some points, such as the elementary cross sections and the inelastic processes. As in ref. [40]), we observe that the entropy produced does not allow to reach the critical point and is, anyway, smaller than the "empirical" value (we put quotation marks because it is not clear that the entropy can be extracted from experiments reliably), which turns out to be about the same in ($\lesssim$1 GeV) proton induced reactions [40,49]) and in medium energy heavy ion reactions [50]). As explained in refs. [42,48]), extra entropy can be gained by phase separation, by mechanical instability [46]), cluster formation [40]), surface excitation, and so on.

8. Conclusion

With the help of an INC model we have studied the interaction between an incoming proton and a nucleus in the energy range from ~100 MeV and ~20 GeV. We have seen that the collison process can be divided into three stages. In the first one, the incident proton propagates along roughly a straight line, through the nucleus, losing some energy by a few primary collisions. In the second stage, the nucleus emits a few fast nucleons. The latter are either the nucleons which have been hit in the primary collision or those which are involved in the secondary collisions. The third stage is akin a usual evaporation stage, where the nucleus emits a few slow nucleons. This process obviously involves nucleons which make many collisions. The INC model used here is adequate for the description of the first two stages, dominated by rather hard collisions. Although the model can reproduce emission of slow particles, it is however not realistic enough for providing a good description of this process.

We have paid particular attention to the energy loss of the incident proton and to the associated quantities like the number of primary collisions (and their fluctuations), the energy loss per collision, the transverse motion, ... The main mechanism for the energy loss is the elastic nucleon-nucleon scattering and the excitation of the Δ-resonance. The latter is the most efficient, even though the pion production (coming from the decay of the Δ-resonances) is not very important. As a by-product of our calculation, we calculate the nuclear stopping power in the whole energy range under consideration.

We also studied the properties of the ejected particles and especially of the emitted fast (or grey) particles, although in our model the definition of these particles is not very precise. We paid particular attention to the relationship between the number

of grey particles and the number of primary collisions, apparently a key concept to understand particle production at high energy. We have shown that the relationship is linear to a good approximation, irrespective of the incident energy (at least in the domain under consideration). It is not universal however, since there is a slight dependence upon the size of the target. This relationship seems to be roughly consistent with the results at higher energies (several hundreds of GeV), which have been extensively studied. However, in our opinion this agreement is accidental, as the energy loss mechanism is not the same. At high energy, the main mechanism is the abundant and unconstrained pion production (since the energy necessary to produce a pion is negligible compared to the available energy). In the energy domain studied here, the main mechanism is the delta excitation, for which the required energy is not small at all in comparison with the available energy.

One of the motivations for this work was the detailed study of the energy deposition mechanism, for which the usual fragmentation models are generally using rather crude assumptions. Percolation models as we said, assume that the incident particles extract a certain number of nucleons, creating in a sense some voids inside the nuclear medium. Basically, these models describe a direct relation between the fragmentation pattern and the number of voids. We have tried to establish the connection between our INC model and the number of voids. In the simplest approach, it can be taken as the number of fast ejectiles. We have shown that the number of voids is not very large in general and that only fluctuations allow this number to be larger than the critical value, under which these models predict multifragmentation to occur, namely a fragmentation in many pieces, all much smaller than the original target. Further study is necessary however to determine whether the whole picture of ejection of fast particles, as described here, followed by a percolation scenario is capable of describing the experimental data.

We have also tried to establish the possible relationship between our INC model and the liquid-gas phase transition picture of the fragmentation, following the same reasoning as in ref. [40]). We can in our model follow the representative point of the target in the excitation energy per particle-entropy per particle plane. In many cases the representative point spent a relatively long time in the coexistence zone, before coming back to the liquid phase. What happens thermodynamically during such a transformation (and which is not contained in our model) is not clear, but does not seem to be in favorur of a multifragmentation process. On the other hand, in central collisions at least, the representative point enters the instability zone, beyond either the isothermal or the isoentropic spinodals. So, there is a good chance for the system to break into pieces because of the onset of instability. The appropriate description of the latter is beyond our model, since it really involves the interaction energy. This seems to be a viable scenario, since the entropy generated by the hard collisions (soft collisions are very inefficient from this point of view) is smaller than what is indicated by experiment. Further investigations of the link between the early stages of the collisions, embodying an off-thermal equilibration and the later stages where

thermodynamical considerations are becoming more and more relevant are certainly necessary.

We are very grateful to Dr. X. Campi for his continuous encouragement and for fruitful discussions. We also thank Dr. Madeleine Soyeur for her enthusiastic comments and Dr. Denis L'Hôte for his criticisms.

References

1) P. Schwandt, The interaction between medium energy nucleons in nuclei, ed. H.O. Meyer (AIP Editions, 1983) p. 89
2) G.W. Hoffmann *et al.*, Phys. Rev. **C24** (1981) 541
3) J.M. Cameron, Nucl. Phys. **A434** (1985) 261c
4) G. English, N.T. Porile and E.P. Steinberg, Phys. Rev. **C10** (1974) 2268
5) G. Rudstam, Z. Naturforsch. **21a** (1966) 1027
6) G. Fai and J. Randrup, Nucl. Phys. **A381** (1982) 557
7) D.H.E. Gross *et al.*, Z. Phys. **A309** (1982) 41
8) J. Aichelin and J. Hüfner, Phys. Lett. **136B** (1984) 15
9) M.E. Fisher, Physica **3** (1967) 225
10) A.D. Panagiotou *et al.*, Phys. Rev. Lett. **52** (1984) 496
11) R.W. Minich *et al.*, Phys. Lett. **118B** (1982) 458
12) W. Bauer *et al.*, Phys. Lett. **150B** (1985) 53; Nucl. Phys. **A452** (1986) 699
13) X. Campi and J. Desbois, Seventh high energy heavy ion study, GSI Publication GSI-85-10 (1985) 707
14) T.S. Biro, J. Knoll and J. Richert, Nucl. Phys. **A459** (1986) 692
15) J. Cugnon, Heavy ion collisions, ed. P. Bonche, M. Lévy, P. Quentin and D. Vautherin (Plenum, London, 1986) p. 209.
16) J. Cugnon and J. Vandermeulen, Nucl. Phys. **A445** (1985) 717
17) J. Cugnon, D. Kinet and J. Vandermeulen, Nucl. Phys. **A379** (1982) 553
18) Particle Data Group, NN and ND interactions (above 0.5 GeV/c). A compilation, UCRL-20000NN, 1970
19) G. Bizard *et al.*, Nucl. Phys. **B108** (1976) 184
20) A. Rittenberg *et al.*, Part. Data Group, Rev. Mod. Phys. **43** (1971) S114
21) G. Bertsch and J. Cugnon, Phys. Rev. **C24** (1981) 2514
22) T.A. Shibata *et al.*, Nucl. Phys. **A408** (1983) 525
23) K. Nakai *et al.*, Phys. Lett. **121B** (1983) 373
24) K. Nakai *et al.*, preprint UTPN-175
25) H. En'yo, Doctoral thesis, University of Tokyo, 1985
26) M. Soyeur, Proc. of the second Int. Workshop on Local equilibrium in strong interactions physics, Santa Fé, USA, April 1986, to be publshed
27) J. Cugnon, T. Mizutani and J. Vandermeulen, Nucl. Phys. **A352** (1981) 505
28) H. Meyer, M.W. Teucher and E. Lohrmann, Nuovo Cim. 27 (1963) 2945
29) Tsai-Chü *et al.*, Lett. Nuovo Cim. **20** N.8 (1977) 257.
30) I. Otterlund *et al.*, Nucl. Phys. **B142** (1978) 445.
31) B. Andersson *et al.*, Nucl. Phys. **B191** (1981) 173.
32) E. Stenlund and I. Otterlund, Nucl. Phys. **B198** (1982) 407.
33) M. Baldo and O. Civitarese, Nuclear structure and heavy ion collisions (North-Holland, Amsterdam 1981) p. 604
34) B. Andersson, I. Otterlund and E. Stenlund, Phys. Lett. **74B** (1978) 343
35) D. Stauffer, Phys. Reports **54** (1979) 1
36) J. Aichelin and X. Campi, preprint, Orsay IPNO/TH 86-21, 1986
37) C.J. Waddington and P.S. Freier, Phys. Rev. **C31** (1985) 888

38) A.L. Goodman, J.I. Kapusta and A.Z. Mekjian, Phys. Rev. **C30** (1984) 851
39) L.P. Csernai, Phys. Rev. Lett. **54** (1985) 639
40) D.H. Boal and A.L. Goodman, Phys. Rev. **C33** (1986) 1690
41) D.H. Boal, contribution to the RHIC Workshop, Brookhaven National Laboratory, April 1986
42) J.A. Lopez and P.J. Siemens, Nucl. Phys. **A341** (1984) 728
54) G. Bertsch and P.J. Siemens, Phys. Lett. **126B** (1983) 9
44) H. Schultz *et al.*, Phys. Lett. **147B** (1984) 17
45) H.W. Barz *et al.*, Nucl. Phys. **A448** (1986) 753
46) J. Cugnon, Phys. Lett. **135B** (1984) 374
47) B. Strack and J. Knoll, Z. Phys. **A315** (1984) 249
48) L.P. Csernai and J.I. Kapusta, Phys. Reports **131** (1986) 223
49) R.E.L. Green, R.G. Korteling and K.P. Jackson, Phys. Rev. **C29** (1984) 1806
50) B.V. Jacak *et al.*, Phys. Rev. Lett. **51** (1983) 1846
51) X. Campi, private communication